Conformational distribution of the potentially neurotoxic metabolite of haloperidol, HPP^+, by NMR spectroscopy, X-ray crystallography and molecular dynamics simulations

Frederic Ooms,*[a] Johan Wouters,[a] Francois Durant,[a] Neal Castagnoli, Jr.,[b] Clinton Van't Land,[b] Gisella Dockendolf,[c] Thomas Glass[b] and Cornelis J. Van der Schyf †[b,c]

[a] *Laboratoire de Chimie Moleculaire Structurale, Facultés Universitaires Notre-Dame de la Paix, Namur, Belgium*
[b] *Department of Chemistry and the Harvey W. Peters Center for the Study of Parkinson's Disease and Disorders of the Central Nervous System, Virginia Polytechnic Institute and State University, Blacksburg, VA 24061, USA*
[c] *Department of Pharmaceutical Chemistry, Potchefstroom University for Christian Higher Education, Potchefstroom 2520, South Africa*

In order to gain more insight into the mechanisms underlying mitochondrial inhibition by haloperidol (HP) pyridinium metabolites, we have studied the three dimensional structure of these compounds. In this paper we report the results of experimental (NMR studies in solution, X-ray diffraction) and theoretical methods (molecular dynamics) applied to HPP^+. The chlorophenyl and pyridinium rings are found not to be strictly coplanar and a high degree of mobility was observed in the butyroxy chain. Calculations have shown that the most stable structures adopt conformations corresponding to either *gauche* or *trans* rotamers. From these data, a model for the interaction of HPP^+ with electron transfer complexes in the mitochondrial respiratory chain has been proposed.

Introduction

Haloperidol, 4-[4-(4-chlorophenyl)-4-hydroxypiperidino]-4′-fluorobutyrophenone (HP, **1**), a member of the butyrophenone

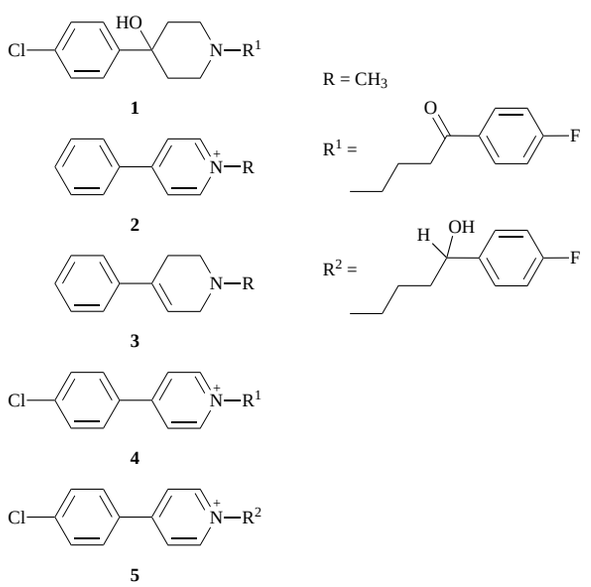

class of neuroleptics, is one of the most widely prescribed drugs used in the treatment of acute and chronic psychotic disorders. The typical neuroleptic drugs, including HP, form the mainstay of pharmacotherapeutic treatment of schizophrenia.[1] Moreover, DesJarlais *et al.*[2] also found that HP inhibits HIV-1 and HIV-2 proteases in a concentration-dependent manner. Based on these initial findings, stable, non-peptide inhibitors of HIV protease were developed from the HP lead[3] and efforts using computational techniques to optimize the pharmacological profile of HP-derived HIV protease inhibitors are still being pursued.[4] Restricting their wider clinical application in psychiatry and exploitation of the promising HIV protease inhibiting effects is the fact that HP and other typical neuroleptics produce a variety of acute and chronic neurological disorders, including tardive dyskinesia (TD), a potentially irreversible syndrome of abnormal movements affecting in particular the orofacial musculature.[5] Some post-mortem studies in human brain have suggested an association between TD and neuronal damage,[6] but it is generally accepted that conventional neuropathologic examination of the human brain does not reveal any gross lesions in patients with TD. Animal studies have revealed subtle abnormalities in the brain ultrastructure after treatment with neuroleptics,[7–14] but finding unambiguous human neuropathological correlations with TD remains elusive.

Roberts *et al.*[15] treated rats with HP for six months and compared the differences in neuronal ultrastructure between rats that developed a low or high number of vacuous chewing movements (VCMs), which are used as an indicator of TD, and untreated controls. Detailed examination of the mitochondria in the high VCM group revealed that they were reduced in number and that those remaining were hypertrophied. These findings suggest that HP produces neuronal toxicity; that this is probably mediated by its pyridinium metabolites; and that these metabolites inhibit mitochondrial respiration in a manner similar to the structurally related pyridinium neurotoxic metabolite, 1-methyl-4-phenylpyridinium, (MPP^+, **2**) of the well-established pro-toxin, 1-methyl-4-phenyl-1,2,3,6-tetrahydropyridine (MPTP, **3**).

We and others have demonstrated[16–18] that HP is metabolized to the pyridinium species 4-(4-chlorophenyl)-1-[4-(4-fluorophenyl)-4-oxobutyl]pyridinium (HPP^+, **4**) in rodents and have

† Present address: Department of Biomedical Sciences and Pathobiology, VA-MD Regional College of Veterinary Medicine, Virginia Polytechnic Institute and State University, Blacksburg, VA 24061, USA.

Table 1 Crystallographic data, data collection and refinement parameters for HPP^+Cl^- [a]

Crystallographic data	
Molecular formula	3 $[(C_{21}H_{18}NOClF)^+Cl^-]\cdot 6H_2O$
Molecular weight	1266.79
Crystal size/mm	0.28 × 0.1 × 0.07
Crystal system	Triclinic
Space group	*P*-1
a, *b*, *c*/Å	8.201(3), 18.260(3), 21.024(4)
a, *β*, *γ*/°	83.43(2), 89.60(2), 87.39(2)
V/Å^3	3124.4(14)
Z	2
D(calc)/g cm^{-3}	1.347
F(000)	1308
μ(Cu-K*α*)/mm^{-2}	3.07
Data collection	
T/K	293(2)
λ (Cu-K*α*)/Å	1.541 79
θ range for data collection	2.72–71.91
θ range for refinement	2.72–58.85
Scan type	*ω*/2*θ*
Reference reflections	3 (each hour)
Reflections collected	14 418
Independent reflections	8959 (0.9 Å resolution)
R(int)	0.0341
Observed data [I > 2*σ*(*I*)]	5133
Refinement	
Refinement method	Full-matrix least-squares on F^2
Data/restraints/parameters	8959/189/758
Goof on F^2	1.288
Final *R*1 [*I* > 2*σ*(I)]	0.1046
Final *R*1 (all merged data)	0.1491
*wR*2	0.3594
$w = w_{calc} = 1/[s^2(F_o^2) + (0.200P)^2 + 0.0000P]$	where $P = (F_o^2 + 2F_c^2)/3$
$\Delta\sigma_{max}$/e Å^{-3}	0.200
$\Delta\rho_{max}$/e Å^{-3}	0.970
$\Delta\rho_{min}$/e Å^{-3}	−0.840
Extinction correction	SHELXL
Extinction coefficient	0.0019(5)

[a] Atomic scattering factors from International Tables, vol C, Tables 4.2.6.8 and 6.1.1.4.

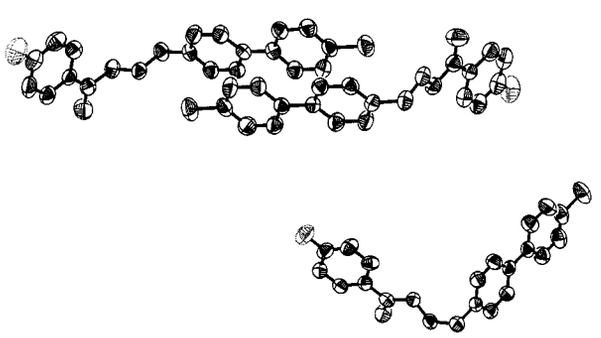

Fig. 1 View of the crystal conformation of HPP^+Cl^- observed in the solid state

also reported on the conversion of HP to HPP^+[19] and a second more major species, 4-(4-chlorophenyl)-1-[4-(4-fluorophenyl)-4-hydroxybutyl]pyridinium ($RHPP^+$, **5**) in humans[20] and baboons.[21] HPP^+ was found to be more potent than MPP^+ as an inhibitor at Complex I (NADH dehydrogenase) of the mitochondrial electron transport chain[22] and also to be a potent neurotoxin.[23] Very recently, we also reported the presence of a urinary biochemical profile indicative of inhibition of mitochondrial respiration in the periphery, in baboons treated with the tetrahydropyridine analog of HP, HPTP.[24]

In an effort to correlate the structure of pyridinium compounds with inhibition of mitochondrial respiration, Nicklas and co-workers[25–27] studied a series of 4-alkylated analogues of MPP^+. The potencies of these compounds correlated with their ability to partition between octan-1-ol and water. In mitochondria, increased hydrophobicity resulted in greater inhibition of Complex I. Furthermore, the pyridinium charge was found to play a major role in the inhibitory mechanism of the pyridiniums because the potencies of these compounds were found to be much greater than would be predicted based solely on hydrophobicity.[28–30] Very little is known about the molecular conformation of HP pyridinium metabolites. It has been demonstrated that flexible bioactive molecules may adopt conformations in the solid state which are usually held only in aqueous medium through the process of hydrophobic collapse.[31] Due to their flexibility and the possibility of undergoing hydrophobically induced folding,[32] the pyridinium metabolites of HP warrant study of their conformations in the solid state and in solution in an effort to better understand their interactions with electron transfer complexes in the mitochondrial respiratory chain. Our present work details the conformational properties of HPP^+. Initiating the study from the crystallographic data obtained from the X-ray structure and the Cambridge Structural Database (CSD),[33] the conformational space of HPP^+ was explored further by high temperature molecular dynamics computations using structural information from ^{1}H NMR and 2D-NOESY measurements.

Table 2 Main torsion angles for the three conformations of HPP^+ with esds in parentheses, for the definition of torsion angles see Fig. 2

Angle	mol 100	mol 200	mol 300
T1	95.7(7)	85.8(7)	87.1(7)
T2	−178.7(5)	−76.9(6)	−77.8(7)
T3	180.0(6)	−172.5(5)	−174.5(5)
T4	77.2(7)	168.5(5)	166.5(5)
T5	−6.1(10)	4.6(10)	−1.5(10)

Results

X-Ray analysis

In the crystal structure, the asymmetric unit contains three HPP^+ ions (Table 1 and Fig. 1) and three chloride counterions. Six additional water molecules were located by difference Fourier maps and included in the final structure. Two ions (200 and 300) adopt almost identical conformations while the third (100) is different. The differences in conformations were underscored by major changes in the torsion angles of the butyryl chain of the molecules (Table 2).

In all three HPP^+ ions, the chlorophenyl rings were found to be coplanar to the pyridinium ring with the carbonyl group projecting in the plane of the terminal fluorophenyl ring (Table 2). This coplanarity in the crystal structure may be explained in terms of packing constraints forcing both rings to orient in the same plane, allowing optimal stacking of the molecules in the crystal. An example of this phenomenon occurs in the biphenyl substructure, which roughly corresponds to the phenyl–pyridyl linkage in HP. The biphenyl fragments tend to crystallize in an approximately planar geometry when there are no substituents in the *ortho*-position,[34] despite the fact that the inter-ring dihedral angle in biphenyl in the vapor phase is reported to be 44°.[35]

These data already suggest considerable flexibility in HPP^+. Indeed, the flexibility of this compound may be rationalized by the presence of a number of equi-energetic conformations corresponding to stable rotamers around the butyryl chain. In solution the coexistence of several conformations of the molecule may be expected to become even more prevalent.

CSD statistical analysis of fragment conformations

To examine the coexistence of several conformations of HPP^+, the distribution of torsion angles T2, T3, T4 of the *p*-butyrophenone (Fig. 2, fragment **I**) derivatives were analyzed. To describe the different side-chains, the conformations were named using the system of classification defined by Kyne and Prelog.[36]

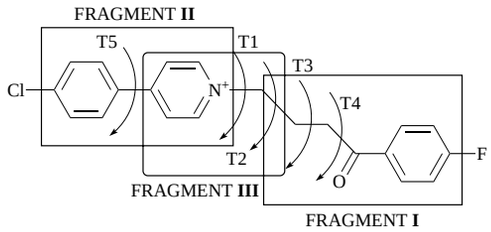

Fig. 2 Fragment designation of the planar structure of HPP^+ used in the CSD search

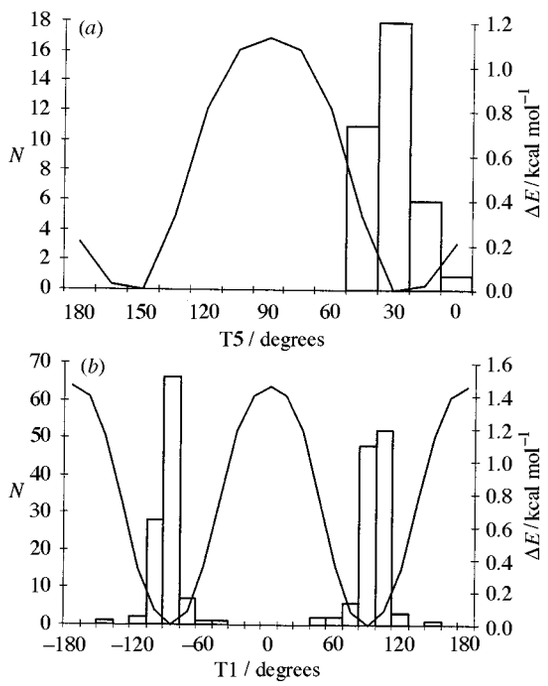

Fig. 3(*a*) Frequency of observation of T5 in CSD. The REF codes and the main characteristics of distribution are available as supplementary material from the authors. Since T5 represents a system with the C_{2v} symmetry, this angle is reported as asin{abs[sin(T5)]}. (□) CSD; (—) cff91. (*b*) Frequency of observation of T1 in CSD. The REF codes and the main characteristics of distribution are available as supplementary material from the authors. (□) CSD; (—) cff91.

Note that this CSD search is biased by the limited structural diversity of the entries containing the fragment **I**. MD simulations have been used to overcome the biases of this fragmental approach.

Analysis of fragment **II** (Fig. 2) led to the identification of 36 conformational sets. The observed frequency of T5 established that sets containing approximately a 30° (or symmetry related) torsion angle represented the most prevalent conformation [Fig. 3(*a*)]. Note that an extended search of the CSD allowing for coordination of this ligand to metals yields 129 observations with a mean at 24°.

These results differ from those observed in the X-ray structure of HPP^+ where the coplanarity between the chlorophenyl and the pyridinium rings is more marked, with the inter-ring torsion angle approaching 0°.

Analysis of the *N*-alkyl-substituted pyridinium fragment (Fig. 2, fragment **III**) led to the identification of 50 conformational sets. The T1 observation frequency established a preferred conformation at T1 ≈ 90° [Fig. 3(*b*)].

NMR results

We examined the conformational properties of HPP^+ in solution using NMR spectroscopy with CD_3OD as solvent. The ^1H and ^{13}C NMR signals of HPP^+ assigned and chemical shifts and coupling constants are given in Table 3.

Through-space interactions in molecules were established by 2D-NOESY measurements. This proved particularly helpful

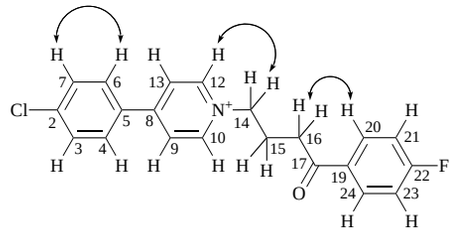

Fig. 4 Through-space interactions observed by NOESY (HPP^+Cl^-·CD_3OD)

Table 3 ^{13}C and ^1H chemical shifts for HPP^+Cl^- in CD_3OD

	Chemical shift[b]		
C/H[a]	δ_C	δ_H	J_{HH}
2	134.20		
3 or 7	131.40	7.83 (d)	8.7
4 or 6	131.11	8.18 (d)	8.7
5	140.12		
8	157.00		
9 or 13	126.46	8.58 (d)	7.0
10 or 12	146.37	9.19 (d)	7.0
14	61.90	4.89 (t)	7.6
15	26.96	2.62 (t)	7.2
16	35.92	3.44 (t)	6.9
17	198.86		
19	134.73		
20 or 24	132.37	8.24 (m)	8.9
21 or 23	116.98	7.40 (t)	8.9
22	167.72		

[a] Atom position numbered as in Fig. 4. [b] Resonance multiplicities are denoted as s, d, t, m for singlet, doublet, triplet and multiplet (ppm with reference to TMS).

where the results of a typical 2D-NOESY experiment not only verified earlier 1D assignments, but also provided important information about the conformation of HPP^+ in solution. The observed through-space interactions for HPP^+ are shown in Fig. 4.

All the through-space interactions confirmed the connectivity assignments made with H,H-COSY. Of considerable interest in the conformational analyses are the 2D-NOESY cross peaks shown for the H16(a,b)–H20(=H24), H14(a,b)–H10(=H12) and H9(=H13)–H4(=H6) protons.

Conformational analysis

During each MD simulation 20 conformers were stored after subsequent minimizations. These simulations were repeated 10 times, using different starting geometries for HPP^+ to generate 200 conformations. All the conformers obtained occurred within a range of 5 kcal mol^{-1} from the lowest energy conformer which had a folded conformation for the bridge chain.

Three geometrical descriptors (Fig. 5) were considered in order to quantitatively probe the conformational space of HPP^+. From these data it is clear that HPP^+ behaves with substantial flexibility.

The most frequently observed torsion angle for T1 was approximately 90° [Fig. 6(*a*)]. The same analysis was performed for torsion angle T5 [Fig. 6(*b*)]. All these sets correspond to the same family of conformers as seen in Fig. 3(*a*) the most observed torsion angle of T5 being, by symmetry, equivalent to the 30° conformation.

A cluster analysis was then performed with the Analysis module of MSI/Biosym.[37] Among the 200 conformers generated by MD, 34 families were defined on the basis of an rms fit (rms < 0.75 Å). The results of the cluster analysis are shown in Table 4. The population of each family is estimated by the number of structures in the family divided by the total number of structures in all families.

From these 34 families, the frequency of observation of the distance *d* between the centroids of the fluorophenyl and pyrid-

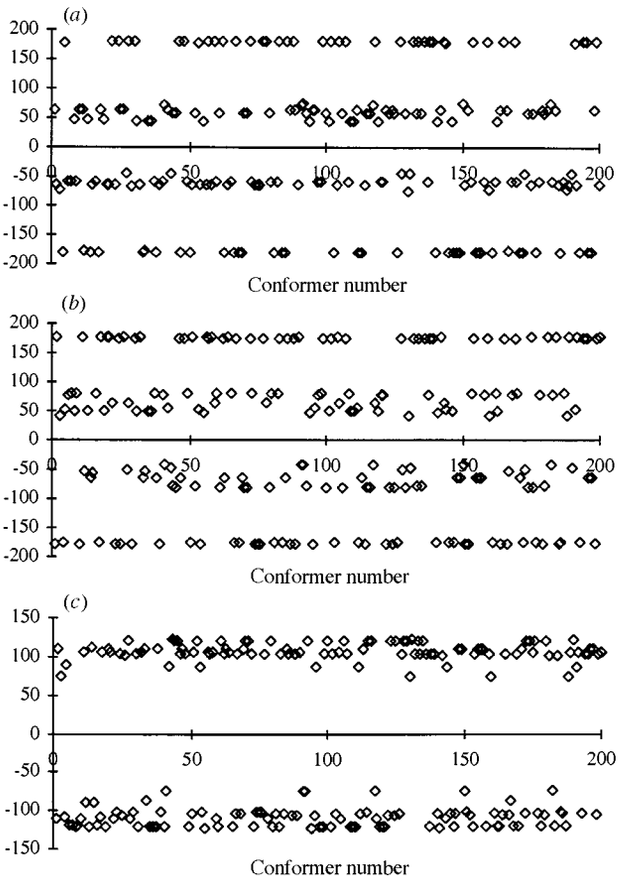

Fig. 5 Range of values explored for the geometrical descriptors T2 (*a*), T3 (*b*) and T4 (*c*) of the butyryl chain during the MD runs simulated in methanol

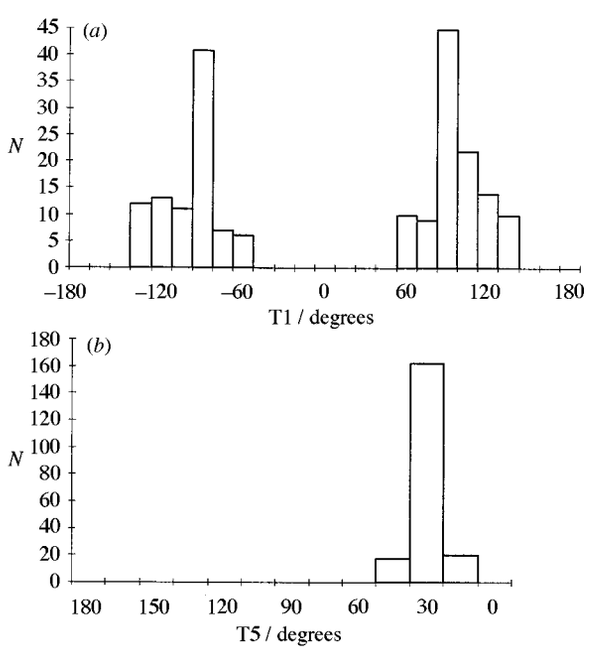

Fig. 6(*a*) Frequency of observation of T1 during MD simulations in methanol. (*b*) Frequency of observation of T5 during MD simulations in methanol. Since T5 represents a system with the C_{2v} symmetry, this angle is reported as asin{abs[sin(T5)]}.

inium rings was studied. This analysis suggested that there are two types of possible conformations, *i.e.* folded ($d < 5$ Å) and unfolded ($d > 6.5$ Å). The ratio of folded to unfolded structures is approximately $\frac{1}{3}$–$\frac{2}{3}$ (Fig. 7). For the folded structures, it was noticeable that the interproton distances between the fluorophenyl and pyridinium rings were less than 5 Å.

Table 4 Population of the families generated by cluster analysis and root conformer geometries

Family no.	T1/°	T2/°	T3/°	T4/°	T5/°	Population (%)
1	−58.0	−59.2	78.1	−118.8	154.8	3.5
2	−117.8	72.8	−41.1	−75.3	16.5	2.0
3	56.5	59.0	−78.6	120.3	−149.5	5.5
4	114.3	−74.2	41.7	75.3	−144.3	1.0
5	118.6	−57.7	79.5	−119.2	−151.1	8.5
6	−102.7	65.1	176.8	105.9	−140.6	1.0
7	58.6	72.7	−41.2	−75.3	23.4	1.0
8	−121.6	59.0	−78.6	120.3	14.9	4.5
9	−61.2	−72.6	41.2	74.6	− 161.8	1.0
10	−50.8	−45.7	−48.6	120.6	145.5	1.5
11	−124.5	46.0	49.3	−120.6	23.8	4.0
12	87.9	177.6	52.9	88.7	156.0	1.0
13	121.9	−43.1	−46.1	122.5	27.7	1.5
14	50.8	45.7	48.6	−120.6	25.3	3.0
15	−88.4	−179.5	−64.9	112.4	24.0	3.5
16	90.7	−179.4	−64.9	110.6	24.1	4.5
17	88.4	179.4	64.9	−110.6	156.5	2.0
18	−90.6	179.4	64.9	−110.6	23.8	1.5
19	−89.1	179.7	175.3	104.2	23.7	7.0
20	89.4	−179.7	−175.3	−108.3	156.1	6.0
21	−89.6	−179.7	−175.2	−108.3	24.0	3.0
22	89.5	179.7	175.3	104.2	156.7	7.0
23	102.7	−65.1	−177.3	−101.2	−153.8	2.0
24	76.4	65.1	176.7	106.0	−155.6	2.0
25	−75.5	−65.2	−177.3	−101.3	−157.9	3.0
26	−102.7	65.1	176.8	105.9	155.5	1.0
27	99.7	−64.1	176.7	105.8	24.2	3.0
28	−79.5	−64.1	176.7	109.3	−24.1	4.0
29	−99.7	64.1	−176.7	−109.3	−156.1	3.0
30	79.2	64.1	−176.6	−105.8	24.2	3.5
31	87.9	177.6	52.9	88.7	156.0	2.0
32	91.3	−177.6	−52.9	−88.6	156.1	1.5
33	−116.9	62.8	55.2	87.3	−23.8	1.0
34	−63.6	−62.9	−55.1	−88.5	−156.1	0.5

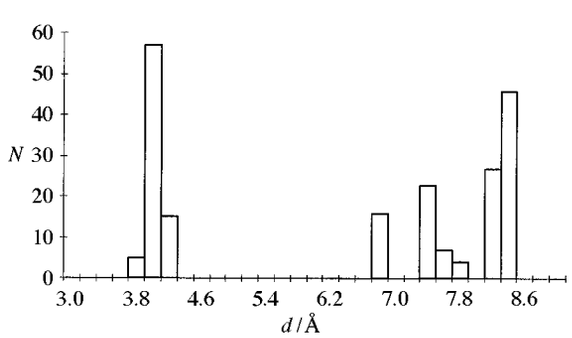

Fig. 7 Observed ratios of occurrence of the folded conformation ($d < 5$ Å, bottom cluster) and unfolded conformation ($d > 6.5$ Å, top cluster) of HPP^+

Discussion

Comparison of conformational preferences derived from the fragment approach and MD simulations

In order to assess the relevance of the high-temperature MD protocol used to study this non-trivial system, the distribution of geometric descriptors obtained from the CSD were compared with those sampled during the MD runs.

The distribution of T5 and T1 derived from the CSD were similar to those explored during the MD simulations. The preferred conformation for torsion angle T1 at 90°, observed both in the CSD and in our MD runs, was in good agreement with recent results obtained at the restricted Hartree–Fock (RHF) level of theory with the 6–31G** basis set for *N*-alkylpyridinium.[38] This study has shown the rotational barriers for *N*-ethylpyridinium and *N*-propylpyridinium to be less than 2.5 kcal mol^{-1} with energy minima for both these structures occurring at 90°. Energy maxima were observed at 0 and 180° and may be attributed to steric interactions between the methy-

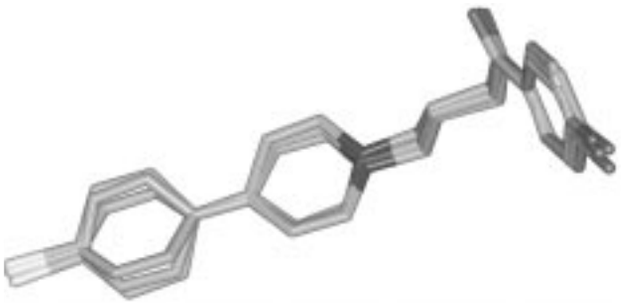

Fig. 8 Structures of the family obtained from the cluster analysis, related to ion 100 (see Fig. 2) observed in the crystal structure

lene groups in the side chains and the hydrogen atoms of the pyridinium ring.

The distribution of torsion angle T5 is also in good agreement with a conformational analysis performed on MPP^+ analogs.[39] That study has shown that the rotation barrier around the inter-ring bond is less than 2.5 kcal mol^{-1} for 4-phenylpyridine derivatives, with the minimum energy structures corresponding to inter-ring torsion angles of 30 and 150°. Recently, we solved the X-ray structure of the 2:1 complex of *N*-cyclopentyl-4-phenylpyridinium bromide (an MPP^+ analog) with 4-phenylpyridine.[40] The observed torsion angle between the phenyl and pyridinium rings was also found to be 30°. Figs. 3(*a*) and (*b*) show that conformational preferences in the crystalline state are significantly correlated with conformational energy differences calculated by molecular mechanics using the cff91 forcefield. These data suggest that cff91 forcefield and the high temperature MD protocol are suitable for the study of pyridinium species such as HPP^+.

Comparison of conformers obtained from MD simulations with experimental results

The torsion angles in the *p*-butyrophenone chain of HPP^+ estimated by MD simulations were compared with those obtained in the X-ray structures. Among the conformations generated for HPP^+, one major family of conformers derived from the cluster analysis was related to one of the molecules (100) observed in the crystal structure. The *p*-butyrophenone chain was characterized by a *trans* (T2 = −179.7°), *trans* (T3 = −173.5°), *gauche* (T4 = −108.4°) configuration (Fig. 8).

Analyses of the NMR spectra and the conformations suggested by the MD runs led us to propose that the preferred conformation of HPP^+ in solution should be unfolded despite the fact that folded conformations usually are lower in energy.[32] No NOESY cross-peaks were observed between the protons of the fluorophenyl and pyridinium rings. The ^1H NMR chemical shift data of the aromatic protons also support an unfolded structure because of a lack of any upfield shifts that may be indicative of ring current shielding (Table 3) and no fluorophenyl-pyridinium stacking was detected for HPP^+ in CD_3OD. An unfolded conformation is also in agreement with findings indicating that the pyridinium charge plays a major role in the inhibitory mechanism.[28–30] Moreover, recent studies performed on isoquinoline derivatives have shown that these compounds are also inhibitors at complex I of the mitochondrial electron transport chain, supporting an argument favoring a coplanar orientation of the chlorophenyl and pyridinium rings, as observed in the X-ray structure, to be the preferred conformation for xenobiotic interactions.[41] From these data, we have defined a hypothetical binding model for HPP^+ that includes an ionic bond and a hydrogen bond (Fig. 9).

Conclusions

Both experimental (NMR studies in solution, X-ray diffraction) and theoretical methods (molecular dynamics runs) were used to study the structure of the neurotoxic pyridinium metabolite (HPP^+) of HP.

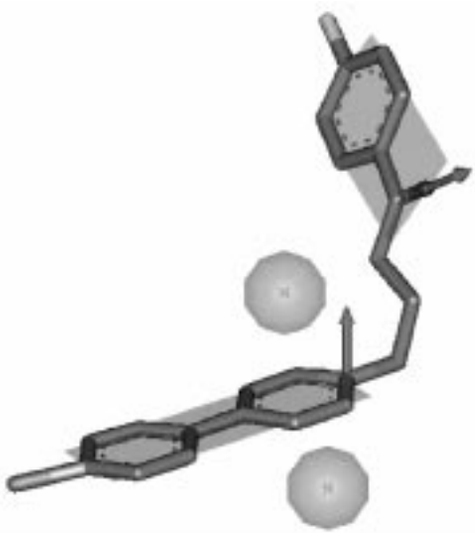

Fig. 9 Proposed binding model of HPP^+ suggesting an ionic bond (A^-–N^+) and an H-bond (HB). Exclusion spheres are shown above and below the pyridinium ring.

It was established that the T1 torsion angle of HPP^+ approaches 90° because this conformation was observed both in crystallography and in the simulated (MD) studies. Several arguments favor a non-strictly coplanar conformation of the chlorophenylpyridinium motif (fragment **II**) in solution. The inter-ring torsion angle (T5) appears to be close to 30°, in contrast with what is observed in the crystal structure where packing constraints not present in solution restrict the angle to near coplanarity.

The flexibility of the butyryl chain of HPP^+ was established and the most stable structures were found to adopt conformations corresponding either to *gauche* or *trans* rotamers. Moreover, the geometries derived from the MD simulations were in reasonable agreement with the NMR and X-ray crystallography data obtained for HPP^+, allowing us to use this methodology in other conformational studies of flexible positively charged conjugated nitrogen-containing compounds such as the reduced form of HPP^+ ($RHPP^+$) which is also a potent neurotoxin.

Experimental

Crystallography

The chloride salt of HPP^+ was synthesized as described elsewhere.[42] Single crystals were obtained at room temperature by slow evaporation of a solution in Bu^{n}OH. All diffraction measurements were performed at 293 K and collected with an Enraf–Nonius CAD-4 diffractometer equipped with a copper anode. The lattice constants are listed with other relevant crystal data in Table 1.‡ A complete data set was collected to a maximum θ limit of 72°, resulting in a total of 14 418 reflections. The data (12 249 unique reflections) were corrected for Lorentz and polarization effects using the in-house program NONIUS93.[43] The structure was solved with SHELXS86.[44]

All non-hydrogen atoms were refined anisotropically using the program SHELXSL93.[45] Hydrogen atoms were calculated at their standard positions and treated in a riding model. Hydrogen atoms were not included on the water molecules. Correction for extinction was introduced in the last steps of the refinement. Due to the poor data: parameter ratio, bond lengths and valence angles were restrained to be approximately equal in the three independant molecules of the asymmetric unit with an effective standard deviation of 0.03 Å using the stereochemical same restraints in SHELXL93. In the final model, the rms devi-

‡ Atomic coordinates, thermal parameters, and bond lengths and angles have been deposited with the Cambridge Crystallographic Data Centre (CCDC). See 'Instructions for Authors', *J. Chem. Soc.*, *Perkin Trans. 2*, Issue 1. Any request to the CCDC for this material should quote the full literature citation and the reference number 188/104.

ation for these restraints was 0.020 Å. No absorption correction was applied to the data.

Statistical analysis of fragment conformations

The planar structure of HPP^+ was divided into three fragments (Fig. 2) which were searched[33] through the Cambridge Structural Database (CSD, vol. 5.12, October 1996). All the fragments were located within the CSD. The hits were submitted to geometrical and statistical analysis in order to derive mean geometries and to identify the most frequently encountered conformations for those fragments. Crystal structures that displayed *R* factors lower than 0.10 were retained. The search was performed only on organic compounds.

NMR spectroscopy

The spectra were acquired on a Varian Unity 400 MHz NMR spectrometer in CD_3OD (Aldrich, atom 99.9% ^2H enriched), observing ^1H and ^{13}C at 399.95 and 100.58 MHz, respectively. All samples were prepared in 5 mm tubes (Wilmad Glass Company, 528-PP grade) and were analyzed at 298 K. The samples were purged with nitrogen gas and the tubes sealed under high vacuum prior to the 2D-NOESY experiments. Spectra were internally referenced to the solvent resonance.

Molecular dynamics

All calculations were carried out using the second generation forcefield cff91 of Maple and co-workers.[46,47] The Discover 95.0 simulation program within Biosym/MSI's Insight II,[37] was used to perform the calculations. Molecular dynamics (MD) were carried out using a relative permittivity (ε) of 32.63 to roughly simulate the conditions under which the NMR data were obtained.

For the first dynamics simulation the X-ray structure (mol 100) was used as the starting conformation and subjected to a 5 ps simulation at 600 K, after which the coordinates were stored and velocities randomized in order to generate a new structure for the next 5 ps simulation. The procedure was repeated 20 times in order to generate 20 structures for a total run of 100 ps. The 20 conformers generated were submitted to an annealing protocol in which the temperature was gradually cooled to 300 K during a 15 ps MD run and then minimized by steepest descent and conjugate gradient to a final RMS gradient of less than 0.001 kcal mol^{-1}. Ten subsequent simulations were performed using as starting conformations other second minimum energy conformations generated in the first run. All the conformations generated in this way were grouped into families of similar structures using the Analysis[37] module of MSI/Biosym. All calculations were performed on the IBM RS-6000 computer system of the Scientific Computing Facility Center of the University of Namur. Each run took about 3 h CPU time.

Acknowledgements

The authors acknowledge IBM Belgium and the Facultés Notre Dame de la Paix for the use of the Namur Scientific Computing Facilities. The authors are also indebted to MSI/Biosym for the use of the beta test version of WebLab Viewer$^+$. J. W. thanks the FNRS for his senior research assistant position.

References

1 D. G. C. Owens, *Drug*, 1996, **51**, 895.
2 R. L. DesJarlais, G. L. Seibel, I. D. Kuntz, P. S. Furth, J. C. Alvarez, P. R. Ortiz de Montellano, D. L. DeCamp, L. M. Babe and C. S. Craik, *Proc. Natl. Acad. Sci. USA*, 1990, **87**, 6644.
3 E. Rutenber, E. B. Fauman, R. J. Keenan, S. Fong, P. S. Furth, P. R. Ortiz de Montellano, E. Meng, I. D. Kuntz, D. L. DeCamp and R. Salto, *J. Biol. Chem.*, 1993, **268**, 15 343.
4 C. M. Oshiro, I. D. Kuntz and J. S. Dixon, *J. Comput.-Aided Mol. Des.*, 1995, **9**, 113.
5 J. M. Kane, M. Woerner and J. Lieberman, in *Dyskinesia Research and Treatment*, ed. D. E. Casey, T. Chase, A. V. Christensen and J. Gerlach, Springer, Berlin, 1985, pp. 72–78.
6 E. Christensen, J. E. Moller and A. Faurbye, *Acta Psychiatr. Scand.*, 1970, **46**, 14.
7 F. M. Benes, P. A. Paskewich and V. B. Domesick, *Science*, 1983, **221**, 969.
8 F. M. Benes, P. A. Paskewich, J. Davidson and V. B. Domesick, *Brain Res.*, 1985, **329**, 265.
9 R. Dom, *Acta Neurol. Pychiatr. Belg.*, 1967, **67**, 755.
10 S. P. Mahadik, H. Laev, A. Korenovsk and S. E. Karpiak, *Biol. Psychiatry*, 1988, **24**, 199.
11 C. K. Meshul and D. E. Casey, *Brain Res.*, 1989, **489**, 338.
12 C. K. Meshul and S. E. Tan, *Synapse*, 1994, **18**, 205.
13 C. K. Meshul, J. F. Buckman, C. Allen, J. P. Riggan and D. J. Feller, *Synapse*, 1996, **22**, 350.
14 C. K. Meshul and S. E. Tan, *Synapse*, 1994, **18**, 205.
15 R. C. Roberts, L. A. Gaither, X-M. Gao, S. M. Kashyap and C. A. Tamminga, *Synapse*, 1995, **20,** 234.
16 B. Subramanyam, H. Rollema, T. Woolf and N, Castagnoli, Jr., *Biochem. Biophys. Res. Commun.*, 1990, **166**, 238.
17 B. Subramanyam, T. Woolf and N. Castagnoli, Jr., *Chem. Res. Toxicol.*, 1991, **4**, 123.
18 C. J. Van der Schyf, K. Castagnoli, E. Usuki, H. G. Fouda, J. M. Rimoldi and N. Castagnoli, Jr., *Chem. Res. Toxicol.*, 1994, **7**, 281.
19 B. Subramanyam, S. M. Pond, D. W. Eyles, H. A. Whiteford, H. G. Fouda and N. Castagnoli, Jr., *Biochem. Biophy. Res. Commun.*, 1991, **181**, 573.
20 D. W. Eyles, H. R. McLennan, A. Jones, J. J. McGrath, T. J. Stedman and S. M. Pond, *Clin. Pharmacol. Ther.*, 1994, **56**, 512.
21 K. M. Avent, E. Usuki, D. W. Eyles, R. Keeve, C. J. Van der Schyf, N. Castagnoli, Jr. and S. M. Pond, *Life Sci.*, 1996, **59**, 1473.
22 H. Rollema, M. Skolnik, J. D'Engelbronner, K. Igarashi, E. Usuki and N. Castagnoli, Jr., *J. Pharmacol. Exp. Ther.*, 1994, **268**, 380.
23 J. Bloomquist, E. King, A. Wright, C. Mytilineou, K. Kimura, K. Castagnoli and N. Castagnoli, Jr., *J. Pharmacol. Exp. Ther.*, 1994, **270**, 822.
24 L. J. Mienie, J. J. Bergh, E. Van Staden, S. J. Steyn, S. M. Pond, N. Castagnoli, Jr. and C. J. Van der Schyf, *Life Sci.*, 1997, **61**, 265.
25 W. J. Nicklas, M. S. Saporito, A. Basma, H. M. Geller and R. E. Heikkila, *Ann. N. Y. Acad. Sci.*, 1992, **648**, 28.
26 M. S. Saporito, R. E. Heikkila, S. K. Youngster, W. J. Nicklas and H. M. Geller, *J. Pharmacol. Exp. Ther.*, 1992, **260**, 1400.
27 M. R. Gluck, S. K. Youngster, R. R. Ramsay, T. P. Singer and W. J. Nicklas, *J. Neurochem.*, 1994, **63**, 655.
28 R. R. Ramsay, J. I. Salach and T. P. Singer, *Biochem. Biophys. Res. Commun.*, 1986, **134**, 743.
29 R. R. Ramsay, J. I. Salach, J. Dadgar and T. P. Singer, *Biochem. Biophys. Res. Commun.*, 1993, **135**, 285.
30 M. R. Gluck, S. K. Youngster, R. R. Ramsay, T. P. Singer and W. J. Nicklas, *J. Neurochem.*, 1994, **63**, 655.
31 Q. Gao and W. L. Parker, *Tetrahedron*, 1996, **52**, 2291.
32 L. F. Newcomb, T. S. Haque and S. H. Gellman, *J. Am. Chem. Soc.*, 1995, **117**, 6509.
33 F. H. Allen, O. Kennard and R. Taylor, *Acc. Chem. Res.*, 1983, **16**, 146.
34 C. P. Brock and R. P. Minton, *J. Am. Chem. Soc.*, 1989, **111**, 4586.
35 A. Almenningen, O. Bastiansen, L. Fernholt, B. N. Cyvin, S. J. Cyvin and S. Samdal, *J. Mol. Struct.* 1985, **128**, 59.
36 W. Klyne and V. Prelog, *Experientia*, 1960, **16**, 521
37 InsightII User Guide 1995, Biosym/Molecular Simulations Inc. San Diego, CA.
38 G. B. McGaughey, E. L. Stewart and J. P. J. Bowen, *J. Comput. Chem.*, 1996, **17**, 1395.
39 C. Altomare, P.-A. Carrupt, N. El Tayar and B. Testa, *Helv. Chim. Acta*, 1991, **74**, 290.
40 J. Wouters, G. Evrard, F. Durant, A. Kalgutkar and N. Castagnoli, Jr., *Acta Crystallogr., Sect. C.*, 1996, **52**, 1033.
41 K. McNaught, U. Thull, P. A. Carrupt, C. Altomare, S. Cellamare, A. Carotti, B. Testa, P. Jenner and D. Marsden, *Biochem. Pharmacol.*, 1996, **51**, 1503.
42 H. Rollema, M. Skolnik, J. D'Engelbronner, K. Igarashi, E. Usuki and N. Castagnoli, Jr., *J. Pharmacol. Exp. Ther.*, 1994, **268**, 380.
43 G. Baudoux and G. Evrard, NONIUS93. Program for Data Reduction, 1993.
44 G. M. Sheldrick, *Acta Crystallogr*., *Sect. A*, 1990, **46**, 467.
45 G. M. Sheldrick, SHELXL93. Program for the Refinement of Crystal Structures, University of Göttingen, Federal Republic of Germany, 1993.
46 J. R. Maple, U. Dinur and A. T. Hagler, *Proc. Natl. Sci. USA*, 1985, **85**, 5350.
47 J. R. Maple, M.-J. Hwang, T. P. Stockfisch, U. Dinur, M. Waldman, C. S. Ewig and A. T. Hagler, *J. Comput. Chem.*, 1994, **15**, 162.

Paper 7/05037B
Received 14*th July* 1997
Accepted 26*th August* 1997